Renewable Energy 36 (2011) 1364–1373

Contents lists available at ScienceDirect

Renewable Energy

journal homepage: www.elsevier.com/locate/renene

Three-dimensional analysis and investigation of the thermal and hydrodynamic behaviors of cylindrical storage tanks

Darci L. Savicki [a,1], Horácio A. Vielmo [a], Arno Krenzinger [b,*]

[a] Mechanical Engineering Department, Federal University of Rio Grande do Sul, Rua Sarmento Leite, 425, 90.170-050 Porto Alegre, Brazil
[b] Materials Engineering Department, Federal University of Rio Grande do Sul, Av. Bento Gonçalves, 9500, Prédio 74 Setor 4, Porto Alegre, RS, Brazil

ARTICLE INFO

Article history:
Received 5 January 2010
Accepted 10 October 2010
Available online 21 December 2010

Keywords:
Storage tanks
Three-dimensional numerical analysis
Finite volume method

ABSTRACT

A numerical analysis of the three-dimensional temperature and velocity fields in horizontal cylindrical storage tanks was performed. The phenomena of laminar natural convection and vertical stratification of temperature were considered. The developed three-dimensional transient computing code solves the equations of energy and momentum through the finite volume method. The simulation of fluid cooling process inside the tank showed the formation of stratified temperature profiles that matched those obtained experimentally. Based on several simulations, a correlation was proposed for determining the degree of thermal stratification inside the tank regarding thermal and geometrical parameters. From this correlation, an expression was proposed to predict the fluid temperature profiles along the time. This information is very important in many applications, such as in thermosiphon solar water heating systems, where the global efficiency of the system increases with the thermal stratification degree of the working fluid. Another case studied considered that the tank was connected to solar collectors, aiming at investigating the influence of the inlet jet position with and without a baffle plate on the preservation of the thermal stratification. Results showed that the baffle plate modified the velocity and temperature fields close to the inlet jet, allowing a better thermal stratification. Also the suitable choice of the inlet jet position allowed the formation of a more effective thermal stratification. Some other aspects of the internal dynamics of this kind of storage tank are presented and discussed. For the cases studied, the inlet jet next to the top led to a greater thermal stratification. However, it was verified that when the inlet jet temperature remains constant for a long period of time, and thus its temperature approaches the temperature of the water inside the tank, for the same height, the temperature profiles obtained become similar to the case of the inlet located at usual height of 2/3 of the diameter.

1. Introduction

One of the issues of interest in natural convection is the optimization of thermal energy storage equipment. An illustrative case is solar water heating systems, in which a good performance of the storage tank represents a considerable increase in the global efficiency. In such systems, one of the most desirable characteristics is an effective thermal stratification. The thermal stratification inside the tank depends on the velocity of the inlet jet as well as on the difference between the inlet and outlet temperatures of the collectors. There are a significant number of studies on the problem of natural convection inside vertical cylindrical cavities, but few works consider horizontal cylindrical cavities. Among the three-dimensional studies, Schneider and Straub [1] investigated numerically the laminar natural convection in inclined cylindrical cavities, in which the top surface temperature was higher than the bottom surface temperature and the side wall was adiabatic.

Eames and Norton [2] studied the influence of the inlet jet on thermal stratification of horizontal cylindrical tanks. They verified that, in the cases in which the hot water jet temperature was time-dependent, a better thermal stratification could be obtained by placing the inlets at different height positions. The use of devices to reduce the velocity of the inlet jet was also suggested. The use of devices such as baffle plates, diffuser tubes or perforated tubes can also be found in studies by other researchers. Alizadeh [3] studied experimentally the charge and discharge processes as well as the influence of different types of diffusers (straight and conic) on the thermal stratification in horizontal tanks. The author found that it

* Corresponding author. Tel.: +55 51 33086841; fax: +55 51 33986841.
E-mail addresses: darcisavicki@furg.br (D.L. Savicki), vielmoh@mecanica.ufrgs.br (H.A. Vielmo), arno.krenzinger@ufrgs.br (A. Krenzinger).
[1] Present address: Instituto de Matemática, Estatística e Física, FURG, Campus Carreiros, Av. Itália, Km 8 Caixa Postal 474 CEP, 96201-900 Rio Grande, RS, Brazil.

0960-1481/$ – see front matter © 2010 Elsevier Ltd. All rights reserved.
doi:10.1016/j.renene.2010.10.011

Nomenclature

A_{ext}	external area of the tank, m^2
c_p	specific heat at constant pressure, kJ/kg K
D	inside diameter of the tank, m
e	thickness, m
g	gravitational acceleration, m/s^2
h_{int}	internal convection heat transfer coefficient, W/m^2 K
h_{ext}	external heat transfer coefficient, W/m^2 K
ℓ	height, m
ℓ^*	normalized height, dimensionless
k	thermal conductivity of the water, W/m K
k_{ins}	thermal conductivity of the insulation, W/m K
m	mass, kg
p	pressure, Pa
r	radius, radial coordinate, m
S	source term, $W/m^3$for energy equation and $kg/m^2 s^2$ for momentum equations
T	temperature, °C
$\overline{T}^*$	mean temperature for normalized profile, dimensionless
T^*	normalized temperature, dimensionless
T_{ini}	initial temperature, °C
T_{int}	mean internal temperature, °C
T_{ext}	external temperature, °C
T_{min}	minimum temperature in the tank, °C
T_{max}	maximum temperature in the tank, °C
ΔT_{ini}	initial temperature difference inside de tank, °C
ΔT_d	thermal stratification degree, °C
t	Time, s
U	overall heat transfer coefficient, W/m^2 K
V	volume, m^3
V_θ	angular direction velocity component, m/s e
V_r	radial direction velocity component, m/s
V_z	axial direction velocity component, m/s
z	axial position, m

Subscripts

d	degree in temperature profile (thermocline)
r	radial direction
z	axial direction
θ	angular direction
int	internal
ext	external
in	inlet
ini	initial
ins	insulation
tot	total
∞	refers to free stream temperature

Superscripts

*	normalized variables

Greek letters

β	coefficient of thermal expansion, K^{-1}
Δ	operator difference
θ	angular direction, rad
μ	viscosity, kg/m s
ρ	density, kg/m^3

can be increased with the use of a divergent conical tube. Zachar et al. [4] studied numerically the impact of a baffle plate facing the inlet jet on thermal stratification in vertical tanks. According to their study, the use of large baffle plates allows the preservation of the thermal stratification, even for high flow rates. Oliveski et al. [5,6] conducted a numerical–experimental investigation in vertical cylindrical tanks, and obtained a satisfactory agreement between the numerical and the experimental results, proposing a correlation for the Nusselt number. Shah and Furbo [7] performed a numerical study about the influence of inlet jets on the temperature stratification in vertical tanks, using a commercial CFD code. It was verified that for high flow rates above 10 l/min a better thermal stratification was obtained using a baffle plate in front of the inlet jet. Consul et al. [8] used parallel computation and a multiblock technique, with structured meshes, to simulate the charge and discharge process (hot water intake) and to investigate the flow influence on the thermal stratification.

The authors of this paper did not find in the literature correlations to describe the transient evolution of thermal stratification in horizontal cylindrical tanks. These correlations are developed in this work. In order to validate the numerical solutions, an experimental apparatus was assembled and several simulations performed. The influence of the insertion of a baffle plate in front of the inlet water jet was also investigated, aiming to enhance the thermocline, thereby expanding the study of Zachar et al [4], who tested this device for vertical cylindrical tanks.

2. Experimental study

The tests were performed to obtain the temperature profile inside the tank during a cooling process, aiming to validate the numerical simulation. Fig. 1a shows this experimental apparatus and Fig. 1b shows a detailed view of the probe with thermocouple distribution.

The inside diameter and length had 0.42 m and 0.57 m, respectively. The internal metallic wall and of the insulation had equal values in the radial and axial directions, being respectively 0.001 m and 0.025 m. The internal metallic wall was made of copper, and the insulation of polyurethane.

The electrical heater was 2500 W and the centrifugal pump 560 W. A temperature probe was built with 20 thermocouples in a vertical arrangement to determine the temperature profiles stratification. Based on this profile, the degree of thermal stratification, defined as the difference between the maximum and the minimum temperature inside the tank [9], could be established.

As shown in many experimental and numerical studies, including those listed in Section 1, the temperature remains practically uniform at horizontal planes. The positions of the thermocouples were chosen based on a previous numerical simulation of the temperature profiles. The highest temperature gradients occur in the lower part of the tank. For this reason, thermocouples were more concentrated in this region, as shown in Fig. 1b.

The thermocouples are J-type (iron-constantan) and have a measuring tip with a diameter of 0.00125 m. Besides the 20 thermocouples, two others were used: one to measure the temperature in the external environment, where the experiments were performed, and another to measure the temperature of the insulation outer surface (facing the environment). The value of temperature in the external environment was used as input data for the numerical simulation, since the boundary conditions for the energy equation are h_{ext} and T_{ext} prescribed. The thermocouple probes are connected to an Agilent data acquisition system, model 34970A, equipped with a 6 ½ digit internal multimeter, a 20

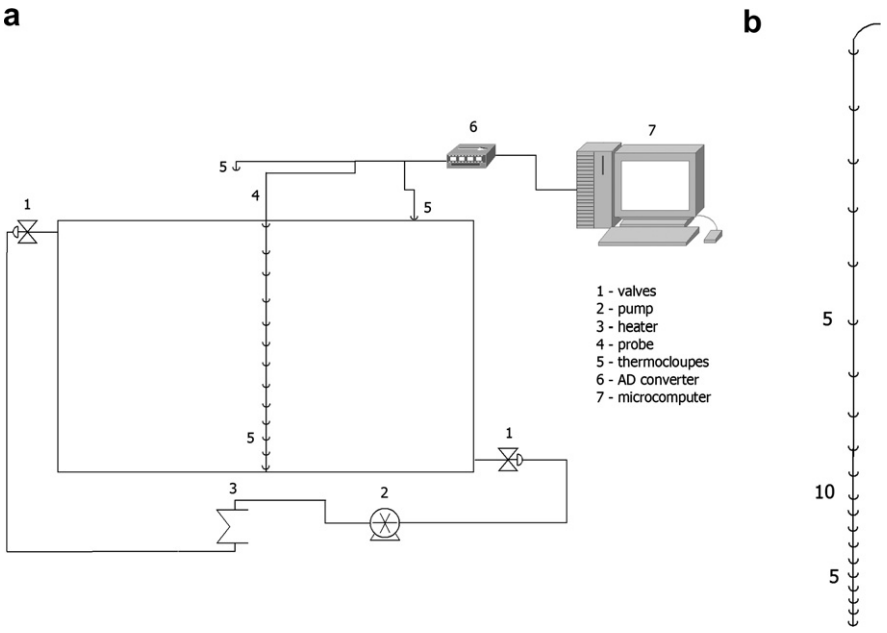

Fig. 1. (a) Experimental apparatus. (b) Detailed view of the probe with thermocouple distribution.

channel multiplexer card with built-in reference junction. As shown in [10], the global uncertainty associated with the experimental measurements was in the order of ±0.3 °C.

In the first experiments the water inside the tank was heated until a specified temperature was reached. Then the temperature was monitored during the cooling process. The temperature measurements were taken with 5-min intervals along 2 days. In later experiments, after reaching the specified temperature, hot water was discharged at constant mass flow from the top of the tank, whereas an identical quantity of cold water was charged through its base. The temperature profiles were also measured along the process. After a predefined volume of cold water was charged and the thermocline formed, the charge/discharge process was interrupted, and the degradation of the thermocline zone was observed by monitoring the temperature profiles. The mass flow rate was determined by measuring the time and volume of the discharged hot water.

3. Mathematical model

For simulations of the cooling process, the calculation domain was just 1/4 of the physical body, assuming two symmetry planes. Furthermore, for simulations with charge and discharge, the calculation domain was just 1/2 of the physical body, considering the symmetry in the plane through the vertical diameter. The inlet and outlet duct diameters are 3/4 in, and are situated at two positions: at 2/3 of diameter and on the top of the tank.

For the determination of the temperature and velocity fields inside the cylindrical horizontal tank, it was necessary to solve the energy and momentum equations in three directions: radial, angular, and axial. In cylindrical coordinates (r, θ, z) and using the Boussinesq approach, for a Newtonian fluid, the problem was described by the following system of equations:

Continuity equation

$$\frac{1}{r}\frac{\partial}{\partial r}(\rho_\infty r V_r) + \frac{1}{r}\frac{\partial}{\partial \theta}(\rho_\infty V_\theta) + \frac{\partial}{\partial z}(\rho_\infty V_z) = 0 \tag{1}$$

where ρ_∞ is the water density calculated at T_{int}.

Momentum equation for the radial velocity component V_r

$$\frac{\partial(\rho_\infty V_r)}{\partial t} + \frac{1}{r}\frac{\partial(\rho_\infty V_\theta V_r)}{\partial \theta} + \frac{\partial(\rho_\infty V_r V_r)}{\partial r} + \frac{\partial(\rho_\infty V_z V_r)}{\partial z} = -\frac{\partial p}{\partial r} + \frac{1}{r^2}\frac{\partial}{\partial \theta}\left(\mu\frac{\partial V_r}{\partial \theta}\right) + \frac{1}{r}\frac{\partial}{\partial r}\left(\frac{\partial(\mu r V_r)}{\partial r}\right) + \frac{\partial}{\partial z}\left(\mu\frac{\partial V_r}{\partial z}\right) + S^{V_r} \tag{2}$$

where μ is the viscosity and the source term is $S^{V_r} = \rho_\infty V_\theta^2/r - (2/r^2)(\partial/\partial\theta)(\mu V_\theta) - \mu V_r/r^2 + \rho\beta(T - T_\infty)g\cos(\theta)$.

Momentum equation for the angular velocity component V_θ

$$\frac{\partial(\rho_\infty V_\theta)}{\partial t} + \frac{1}{r}\frac{\partial(\rho_\infty V_\theta V_\theta)}{\partial \theta} + \frac{\partial(\rho_\infty V_r V_\theta)}{\partial r} + \frac{\partial(\rho_\infty V_z V_\theta)}{\partial z} = -\frac{1}{r}\frac{\partial p}{\partial \theta} + \frac{1}{r^2}\frac{\partial}{\partial \theta}\left(\mu\frac{\partial V_\theta}{\partial \theta}\right) + \frac{1}{r}\frac{\partial}{\partial r}\left(\frac{\partial(\mu r V_\theta)}{\partial r}\right) + \frac{\partial}{\partial z}\left(\mu\frac{\partial V_\theta}{\partial z}\right) + S^{V_\theta} \tag{3}$$

where the source term is $S^{V_\theta} = -\rho_\infty V_r V_\theta/r + (2/r^2)(\partial(\mu V_r)/\partial\theta) - \mu V_\theta/r^2\rho_\infty\beta(T - T_\infty)g\sin(\theta)$, and β is the thermal expansion coefficient.

Momentum equation for the axial velocity component V_z

$$\frac{\partial(\rho_\infty V_z)}{\partial t} + \frac{1}{r}\frac{\partial(\rho_\infty V_\theta V_z)}{\partial \theta} + \frac{\partial(\rho_\infty V_r V_z)}{\partial r} + \frac{\partial(\rho_\infty V_z V_z)}{\partial z} = -\frac{\partial p}{\partial z} + \frac{1}{r}\frac{\partial}{\partial r}\left(\mu r\frac{\partial V_z}{\partial r}\right) + \frac{1}{r^2}\frac{\partial}{\partial \theta}\left(\mu\frac{\partial V_z}{\partial \theta}\right) + \frac{\partial}{\partial z}\left(\mu\frac{\partial V_z}{\partial z}\right) \tag{4}$$

With regard to the problem involving charge and discharge, the initial condition for the momentum was zero velocity in the entire domain. The boundary conditions were zero velocity in the external faces and symmetry conditions on the plane rz, described as $V_\theta = 0; \partial V_r/\partial r = 0$ and $\partial V_z/\partial r = 0$. Along the line $r = 0$, the boundary conditions were $V_\theta = 0; V_r = 0$ and $\partial V_z/\partial r = 0$. The solid domain was kept at zero velocity by the imposition of "infinite" viscosity for this volume. For the case without charge and discharge, there was an additional symmetry plane $r\theta$ in the calculation domain, where symmetry conditions described as $V_z = 0; \partial V_r/\partial z = 0$ and $\partial V_\theta/\partial z = 0$ were also applied.

Energy equation

$$\frac{\partial(\rho_\infty c_p T)}{\partial t}+\frac{1}{r}\frac{\partial(\rho_\infty V_\theta c_p T)}{\partial \theta}+\frac{\partial(\rho_\infty V_r c_p T)}{\partial r}+\frac{\partial(\rho_\infty V_z c_p T)}{\partial z} = \left[\frac{1}{r^2}\frac{\partial}{\partial\theta}\left(k\frac{\partial T}{\partial\theta}\right)+\frac{1}{r}\frac{\partial}{\partial r}\left(kr\frac{\partial T}{\partial r}\right)+\frac{\partial}{\partial z}\left(k\frac{\partial T}{\partial z}\right)\right]+S^T \quad (5)$$

where the term S^T is the source term, also used to incorporate boundary conditions. k and c_p are the thermal conductivity and specific heat at constant pressure of the water, respectively. More details can be found in [11].

For the energy equation, the initial condition was the temperature profile prescribed on the fluid region (in the interior of the tank), and a linear variation between the values T_{ini} (on the internal face) and T_{ext} (on the external face) in thermally insulated region. As boundary condition, symmetry was applied on the plane rz and along the line $r=0$, $\partial T/\partial\theta = 0$ and $\partial T/\partial r = 0$, respectively. On the outer faces of the tank h_{ext} and T_{ext} were prescribed. The boundary conditions for the momentum and energy equations, at the inlet jet, were $V_\theta = 0; V_r = 0; V_z = V_{in}$ and $T = T_{int}$. At the outlet jet, boundary conditions were $V_\theta = 0; V_r = 0; \partial V_z/\partial z = 0$ and $\delta T/\delta z = 0$.

Regarding the case without charge and discharge, for the additional symmetry plane $r\theta$, a symmetry boundary condition was applied, described as $\delta T/\delta z = 0$ for energy equation and $V_\theta/\partial z = 0; V_r/\partial z = 0; V_z = 0$ for momentum equations.

The momentum and energy equations are solved using the finite volume method in cylindrical structured mesh. To solve the algebraic linear equations resulting from the discretization of the governing equations, the TDMA algorithm, with block correction, was employed. The numerical solutions are validated by comparison with experimental data. The Quick advective-diffusive interpolating scheme was implemented, as proposed by Hayase [12] with the extension to non-uniform mesh by Li and Rudmam [13]. In the presence of hot inlet water jets entering the tank, the Quick scheme was observed to produce errors in the volumes near the hot inlet water jet. This fact can be identified by the presence of temperatures with inconsistent physical values (overshoots). This behavior was expected, as typically observed in the application of high order schemes in regions with abrupt gradient changes, such as in this case. For this reason, the Quick scheme was employed only to three-dimensional simulations of the cooling process. For the cases with water circulation, the Power Law scheme was used.

The physical properties of the water (β, ρ_∞, μ, k, c_p) are uniform in space and updated in time, based on the polynomial fitting as a function of water average temperature. The variation in the density in space was considered relevant only in the buoyancy term of the momentum equations. The radiation heat transfer was incorporated in the external convection heat transfer coefficient.

The solution of the transient problem was carried out in a completely implicit form. For each time step, the iterative process was applied until reaching the convergence criterion.

4. Numerical results

For the cooling process without water flow through the tank, it was possible to adopt a computation domain corresponding to 1/4 of the total tank volume. For this domain, the mesh adopted was $40 \times 43 \times 43$ volumes, in the directions θ, r, z, respectively. The adopted time step was 1 s. The convergence criterion was that relative error for temperature and source term for velocity should be less than 10^{-6}.

For the case with charge and discharge of fluid, it was necessary to consider the computation domain shown in Fig. 1a, since symmetry then became restricted to the rz plane. The imposed inlet and outlet boundary conditions took into account that the tank was connected to solar collectors. For this domain, the mesh adopted was $60 \times 45 \times 60$ control volumes, in the directions θ, r, z, respectively. For this case, the time step was reduced to 0.5 s due to the fact that the inlet and outlet jets cause more changes in the velocity and temperature fields.

4.1. Cooling process starting from a uniform temperature field of 50 °C and an environmental temperature of 15 °C

The heat transfer coefficient adopted, experimentally determined as $h_{ext} = 8\ W/m^2\ K$ [10], included losses caused by convection and radiation. For the discretization of the fluid domain, 40 volumes were put in each direction, with a uniform mesh in the angular direction and a non-uniform mesh in the directions r and z. For the internal metallic wall, one volume was used in each direction (radial and axial), and for the insulation wall two volumes were used in each direction. Fig. 2 shows the temperature field, as seen from the symmetry planes obtained from the numerical simulation for 1 h of cooling.

The numerical solution showed a strong stratification at the bottom of the tank as well as the formation of a thermal boundary layer close to the internal faces of the metallic wall. It was also confirmed that the temperature remains constant in horizontal planes along each height, except for the very small thermal boundary layer. This numerical temperature profile agreed with the experimental data, as discussed later. Fig. 3 presents a cross-section of the velocity field in the radial–angular plane, taken approximately at the middle of the tank.

The hydrodynamic boundary layer can be observed in its internal wall face. Furthermore, the existence of recirculation on the top region was observed. Fig. 3b presents a detailed view of this recirculation. The maximum velocity observed in this numerical solution was 0.006 m/s.

4.2. Numerical simulation of cooling process starting from a uniform temperature field of 60 °C and time-dependent environment temperature

This simulation was aimed at reproducing an experimental test in which the initial temperature inside the tank was 60 °C. The

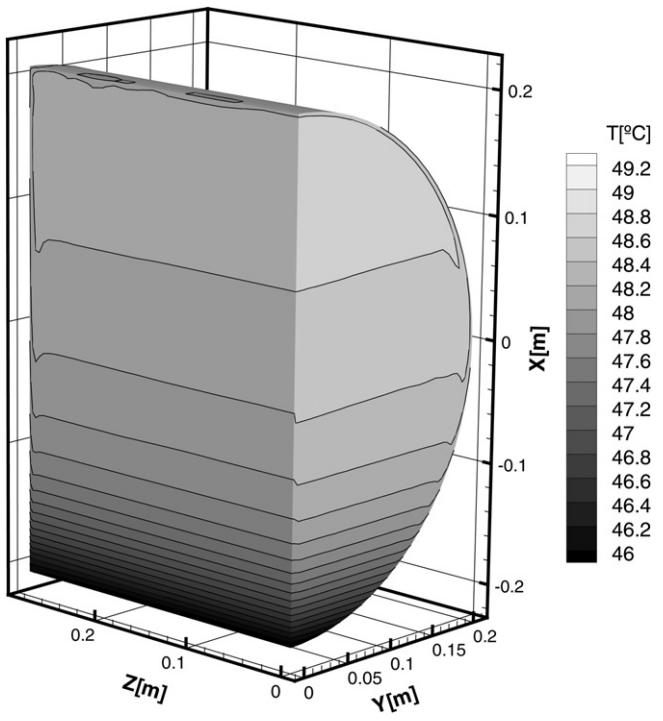

Fig. 2. Temperature field from numerical solution after 1 h of cooling.

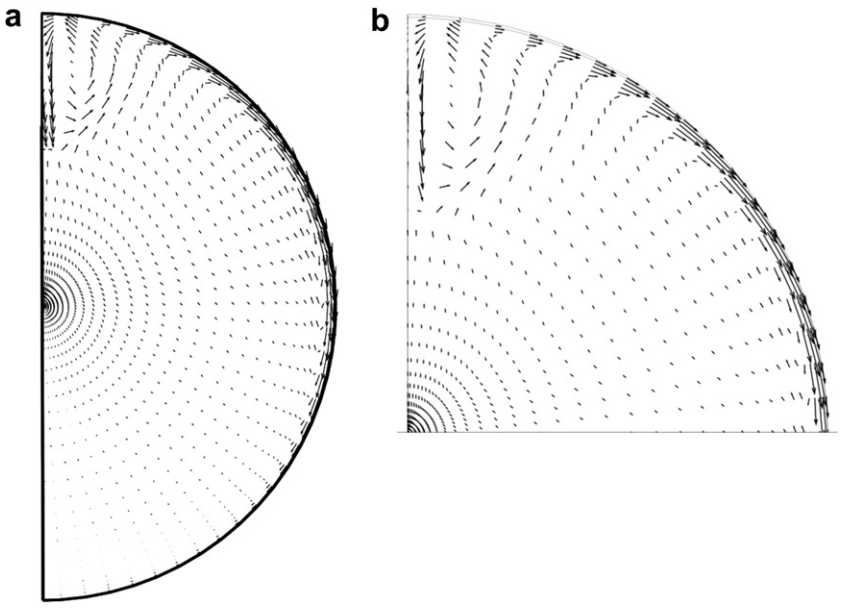

Fig. 3. (a) Velocity field in a cross-section in the middle of tank. (b) Enlarged view of the upper region.

environmental temperature imposed as boundary condition was entered based on the experimental data varying from 22 to 26 °C. Fig. 4 shows a comparison between numerical temperature profiles and experimental data. The error bars represent the experimental uncertainty of ±0.3 °C.

The numerical simulation was able to accurately reproduce the time-dependent cooling process in the tank. The small differences between the experimental data and the numerical results are within the range of uncertainty of the experimental measurements. Besides, part of the difference between the experimental and the numerical profiles can be attributed to the uncertainty of some parameters of the simulation, such as the thickness of the insulation layer and its thermal conductivity.

4.3. Numerical simulation of cooling process starting from an experimental temperature profile with thermocline zone

In this case, the initial temperature field was taken from an experimental profile presenting a thermocline. The objective was to test the numerical code in conditions with more severe thermal gradients, comparing the numerical and experimental temperature profiles.

As shown in Fig. 5, a good level of agreement was obtained between the experimental data and the numerical simulation. For this initial temperature profile, it is possible to observe one point, approximately at the middle of the thermocline zone, where the temperature remains almost constant during the cooling process. This simulation shows that the computational code is able to simulate the natural convection phenomenon, even in the presence of high gradients.

4.4. Correlation for the thermal stratification degree

In order to obtain a correlation for the thermal stratification degree, a large number of simulations were performed, changing the thickness of the insulation layer from 0.02 m to 0.075 m. The water temperature was considered uniform and equal to 60 °C, and the

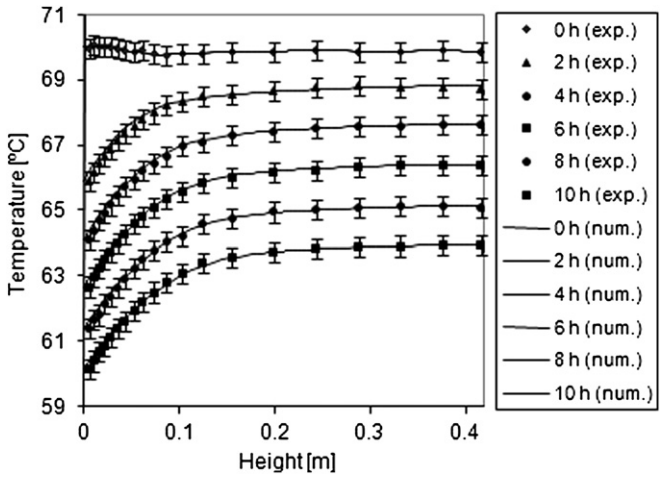

Fig. 4. Comparison between the numerical temperature profiles and experimental data, for the case with initial temperature of 60 °C and variable environmental temperature.

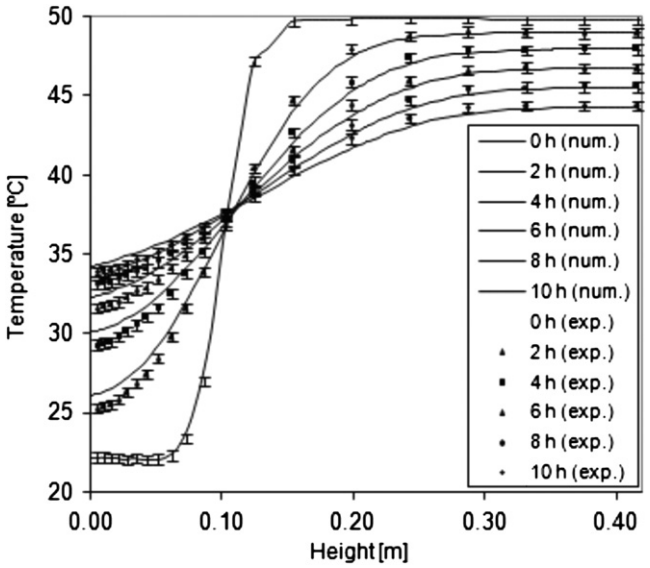

Fig. 5. Comparison between the numerical temperature profiles and experimental data for the case with thermally stratified initial temperature profile.

environment temperature was 20 °C. The adopted heat transfer coefficient was 8 W/m^2 K and the thermal conductivity of the insulation was 0.0305 W/m K. The simulated tank had an internal radius of 0.25 m and an aspect ratio of 1.0. The results showed that even for the same cooling period the stratification degree was larger in cases when the thickness of the insulation layer was reduced. In additional simulations, the thermal stratification degree was verified to increase as the initial temperature difference of the cooling process increased. Fitting the initial temperature difference (ΔT_{ini}), the internal diameter (D) and time (t) from numerical data, based on the overall heat transfer coefficient (U), the following correlation for the thermal stratification degree was obtained:

$$\Delta T_d = (2U+1)\cdot(0.04\Delta T_{ini}+0.25)\cdot\left[\frac{\ln(D/2)}{5}+1.3\right]\cdot [0.5885(1-\exp(-0.5478\,t))] \quad (6)$$

where U is defined as $U = k_{ins}/e_{ins} + h_{ext}$. Here, e_{ins} is the thickness and k_{ins} is the thermal conductivity of the insulation, and A_{ext} is the external area of the tank. The initial temperature difference is defined as $\Delta T_{ini} = T_{ini} - T_{ext}$, and ΔT_d represents the temperature extent.

In Eq. (6), the first term involving U takes into account the influence of thermal resistance. The second term that introduces the variable ΔT_{ini} represents the influence of the initial difference of temperature. The third term considers the physical dimension of the tank, and the last term fits the evolution of the thermal stratification degree along the time.

Fig. 6 gives the transient behavior of the stratification degree ($\Delta T_d = T_{max} - T_{min}$) along the time, for four insulation thicknesses, according to Eq. (6), while Fig. 7 shows the behavior of the stratification degree for four different initial temperatures. In both cases, the correlations profiles are compared with numerical results.

The stratification degree increased more rapidly in the cases when the cooling process was more intense. Also, as it can be observed, the proposed correlation provided profiles that are very well adjusted to numerical results.

In order to obtain an expression for the evolution of temperature profile along the time, two new variables are defined: the normalized temperature (T^*), in the form

$$T^* = \frac{T(\ell) - T_{min}}{\Delta T_d} \quad (7)$$

and the normalized height (ℓ^*), in the usual form

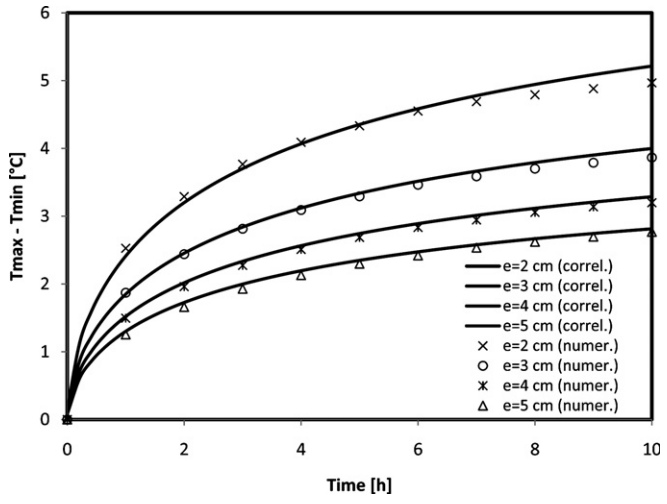

Fig. 6. Time variation of the thermal stratification degree, for different insulation thicknesses (line = correlation; markers = numerical results).

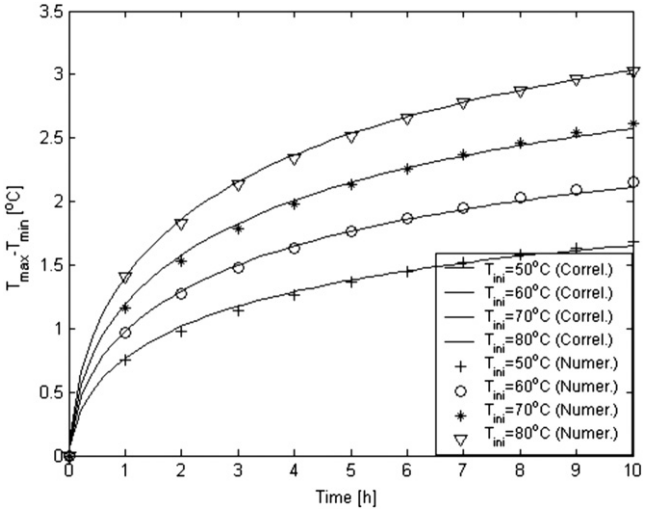

Fig. 7. Time variation of the thermal stratification degree, for different initial temperatures (line = correlation; markers = numerical results).

$$\ell^* = \frac{\ell}{D} \quad (8)$$

Plotting the normalized temperate versus normalized height, the temperature profiles are fitted to a curve, as shown in Fig. 8.

By curve fitting, the normalized temperature profile was described as

$$T^*(\ell^*) = 0.995(1-\exp(-6.4\ell^*) \quad (9)$$

From the definition (Eq. (7)), the temperature profile can be expressed in the form

$$T(\ell) = T^*\Delta T_d + T_{min} \quad (10)$$

The definite integral of Eq. (9), between the normalized height limit 0 and 1, provides

$$\overline{T}^* = \int_0^1 0.995(1-\exp(-6.4\ell^*)d\ell^* \cong 0.84 \quad (11)$$

Integrating Eq. (10) results in

$$\int_0^{2r_{int}} T(\ell)d\ell = \int_0^1 (T^*\cdot\Delta T_d + T_{min})d\ell^* \quad (12)$$

In Eq. (12), the left term of equation can be replaced by

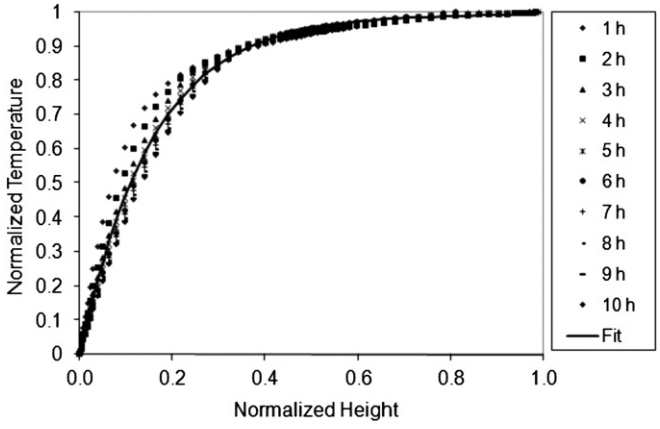

Fig. 8. Curve fitting for normalized temperature as a function of normalized height.

$$T_{int} = \int_0^{2r_{int}} T(\ell)d\ell = (T_{ini} - T_{ext})\exp\left(\frac{t}{-mc_pR_{tot}}\right) \quad (13)$$

So, Eq. (12) can now be expressed as $T_{int} = 0.84 \cdot \Delta T_d + T_{min}$, or, by separating the unknown variable T_{min}, results in the following expression

$$T_{min} = T_{int} - 0.84 \cdot \Delta T_d \quad (14)$$

Finally, returning to Eq. (10), the temperature $T(\ell)$ can now be expressed as

$$T(\ell) = T_{int} + (T^* - 0.84) \cdot \Delta T_d \quad (15)$$

where the variables T^*, T_{int} and ΔT_d are calculated by Eqs. (9) and (13) and correlations for stratification degree, Eq. (6), respectively.

Eq. (15) allows the transient temperature profile to be predicted, since Eqs. (9) and (13) are according to time. Moreover, for any prescribed time, Eq. (15) allows the temperature profile to be described as a function of variables U, ΔT_{ini}, r_{int} and t. Both Eqs. (6) and (15) were applicable with confidence for U in the range 0.4 to 1.3 W/m^2 K, ΔT_{ini} in the range 10–60 °C, r_{int} in the range 0.1–0.3 m, and t from 0 to 36,000 s.

In order to test the validity of this correlation, Fig. 9 shows a comparison between the experimental temperature profiles and those predicted by the correlation, where it is possible to verify the good agreement obtained.

The information provided by the correlation proposed is very important in many solar energy (and other) applications. Moreover, several researches aiming to obtain qualified results in detailed simulations of thermal systems including storage tanks do not have access to experimental results for validating their codes. Using the temperature profile given by this new correlation, it was possible to obtain reference data almost as accurate as actual experimental data, but in a very simpler and economical manner.

4.5. The baffle plate influence on thermal stratification

New simulations were performed considering the connection between the tank and solar collectors, with incorporation of inlet and outlet flows. The simulations were based on a tank with the same dimensions of that utilized in experimental study.

For the inlet jet, velocity and temperature were imposed. For the outlet jet, the global mass conservation to velocity and zero derivative to temperature field were prescribed. The simulations correspond to frequent cases in solar water heating systems, in which the heated water coming from the collectors is delivered on the top of the tank. At the same flow rate, colder water leaves the tank bottom towards the collectors. The goal of these simulations was to expand the understanding on the thermal and hydrodynamic behaviors of tanks connected with solar collectors, besides investigating ways of maximizing the thermal stratification. Hence, cases with and without the baffle plate opposite to the inlet jet were considered, as well as different inlet jet positions and the effect of these variables on the degree of thermal stratification. For these simulations, the water intake temperature was 60 °C, with a flow rate of 0.01667 l/s, at a velocity of 0.0154 m/s. The inlet was located at 2/3 of the diameter. Two cases were considered. In the first one, the water jet entered freely inside the tank. In the second one, the inlet jet was restricted by a facing baffle plate. The baffle plate has approximately a square shape (with the limitations of the polar mesh discretization), with a side of 8 cm. It was installed approximately 1.5 cm ahead of the inner axial face of the tank wall.

Fig. 10 presents a temperature field used as initial condition, with a stratified profile ranging from 50.5 to 55 °C. This profile represents the temperature field after a long period of fluid cooling, taken from experimental data. $h_{ext} = 8$ W/m^2 K and $T_{ext} = 20$ °C were considered as boundary conditions on the external wall.

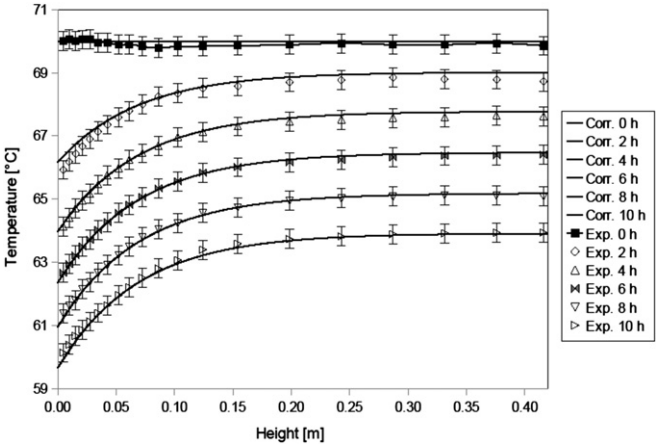

Fig. 9. Comparison between the experimental temperature profiles and those generated by correlation.

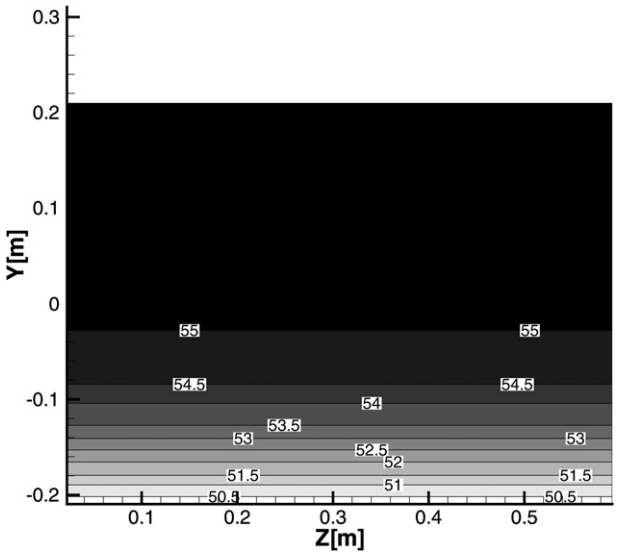

Fig. 10. Stratified temperature field used as initial condition for the numerical simulation.

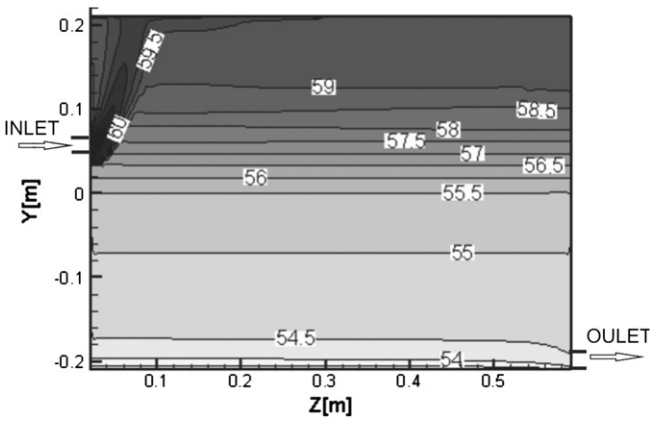

Fig. 11. Temperature field in a symmetry plan in the absence of baffle plate, after the charge of 26 l of water at 60 °C, during 1560 s.

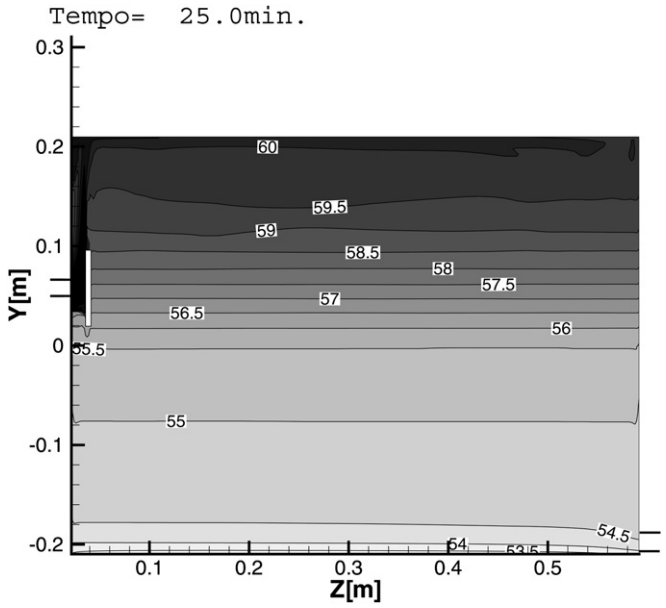

Fig. 12. Temperature field in a symmetry plan in the presence of baffle plate, after the charge of 26 l of water at 60 °C, during 1560 s.

Fig. 11 gives the view of a temperature field of the symmetry plane after the charge of 26 l of water at 60 °C. This volume corresponds to 1/3 of the tank total volume. It is noteworthy that the water present in the upper part of the tank had a temperature lower than the inlet jet temperature. Thus, due to the smaller density, the hottest water takes an ascendant movement towards the top. In most part of the tank, the temperature remained practically constant at the same height, except near the inlet jet, where there is an intense fluid movement and recirculation. This fact caused a more effective mixture between the hot water inlet jet and the pre-existing water in the tank.

In order to preserve thermal stratification, it is desirable to minimize the fluid movement. This can be attempted with the use of a baffle plate facing inlet jet, for example. Fig. 12 shows the temperature profile in the plane *rz*, after the hot water charge of 26 l, for the case with baffle plate. As expected, for this configuration, the incoming water does not mix much with the water already existing inside the tank, thus reaching the top of the tank with a temperature higher than the corresponding case without a baffle plate.

An enlarged view of the inlet jet is shown in Fig. 13. Comparing Fig. 14a and b, one can observe that the baffle plate modified significantly the velocity and the temperature fields near the inlet jet. While in the absence of the baffle plate the jet advanced a distance of approximately 8 cm towards the interior of the tank, with the baffle plate the jet was confined between the internal wall face and the baffle plate, so that it reached the top through a shorter way. Another interesting aspect is that, in both cases, the water velocity increased after entering the tank. This velocity increase was caused by the buoyancy effect. This effect can be evaluated with the velocity magnitude because, while the velocity of the inlet jet was 0.015 m/s, the maximum velocity inside the tank was 0.032 m/s with the baffle plate. The enlarged views shown in Fig. 14 a and b suggest that the dimensions and position of baffle plate can still be optimized, considering that in this study these dimensions and positions were chosen arbitrarily.

Fig. 14 shows a comparison between the numerical prediction for temperature profiles along the height of the tank, taken at the middle point of the axial length, for the cases with and without baffle plate, for every 10 l of hot water flowing into the tank. In the region not disturbed by the inlet jet (the lower part of the tank), there was no significant difference between the profiles but for the upper region, which was disturbed by the inlet jet. The use of a baffle plate led to a greater degree of thermal stratification, identified by higher temperatures next to the top of the tank. These curves have one intersection point at the superior part. In the region under this intersection point, the temperatures for the case with baffle plate are smaller, while in the region above this intersection point they are higher. The presence of this intersection point is an indicative that the use of a baffle plate implies less water mixing.

Fig. 15 extends the last analysis, showing the numerical temperature profiles corresponding to incoming water at 60 °C in

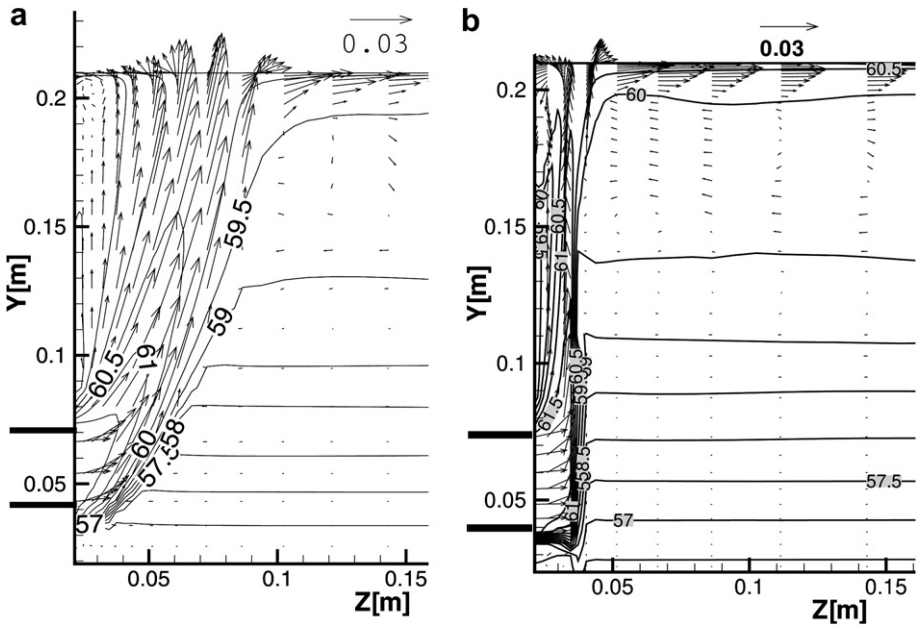

Fig. 13. Detail of the inlet jet region: (a) without baffle plate; and (b) with baffle plate.

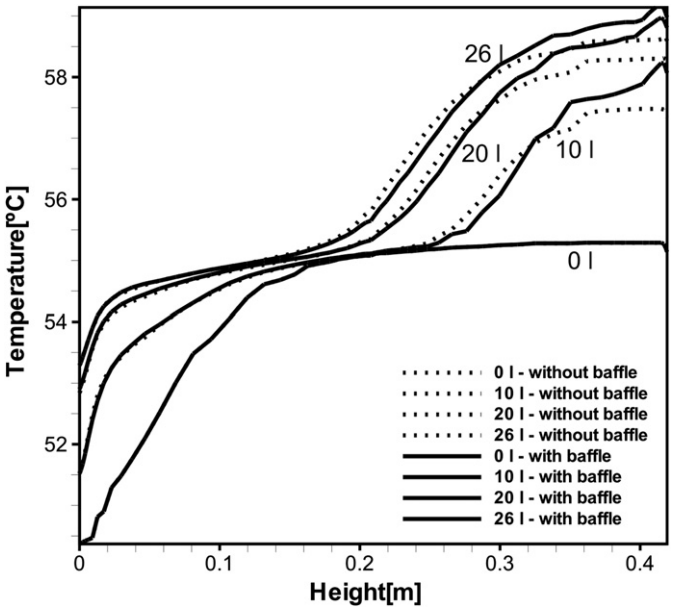

Fig. 14. Comparison of the numerical temperature profiles for the cases with and without baffle plate.

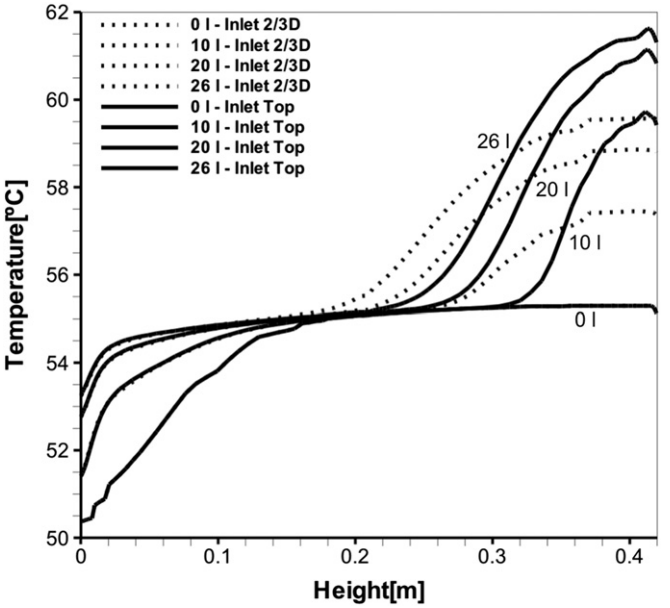

Fig. 16. Comparison of the numerical temperatures profiles for the cases of inlet jets located at 2/3*D* and next to the top, for an intake of 26 l (1/3*V*).

volumes that were equal to 1/3, 2/3, and 3/3 of the total tank volume, that is, 26, 52 and 78 l, respectively.

After the intake of 52 l (2/3*V*) of water, the differences between temperature profiles decreased. After the intake of 78 l, which corresponded to a complete renewal of the water volume in the tank, the temperature profiles for the two cases (with and without the baffle plate) were almost the same. The conclusion is that the baffle plate only improved the thermal stratification when the inlet jet temperature was significantly higher than the temperature of the water in the tank at the jet height. Thus, the gain with the baffle plate can be greater if the difference between the inlet temperature and the tank temperature is increased.

4.6. Storage tank connected to solar collector: influence of the jet position

In the last case, the inlet jet was located at a height of approximately 2/3 of the tank diameter and a baffle plate was used to increase the thermal stratification. Another way of increasing thermal stratification is to select the most adequate position of the inlet jet. Regarding the case presented previously, where the profile of the initial temperature field was stratified in the range of 50.5 to 55 °C, and the inlet jet water temperature was 60 °C, it became clear that the best position for the inlet jet was at the top of the tank. Therefore, new simulations were performed by placing the inlet jet at the top. The initial temperature field was the same

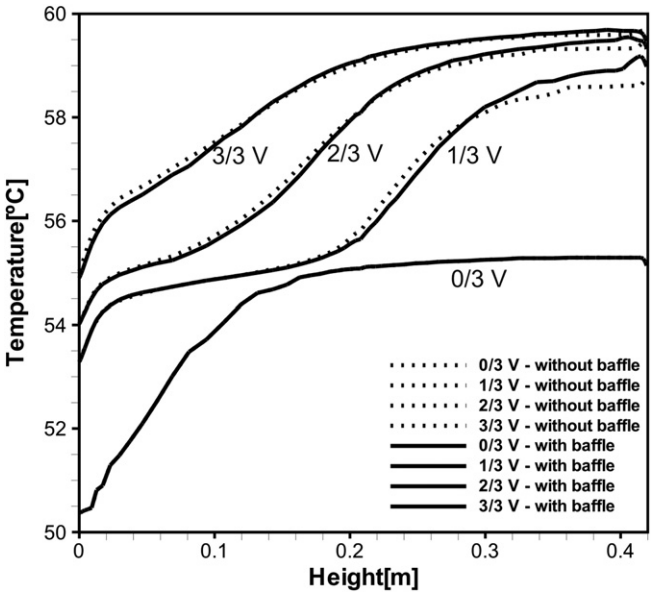

Fig. 15. Numerical temperature profiles for the cases with and without the baffle plate, for water charge of 1/3, 2/3 and 3/3 of the total tank volume.

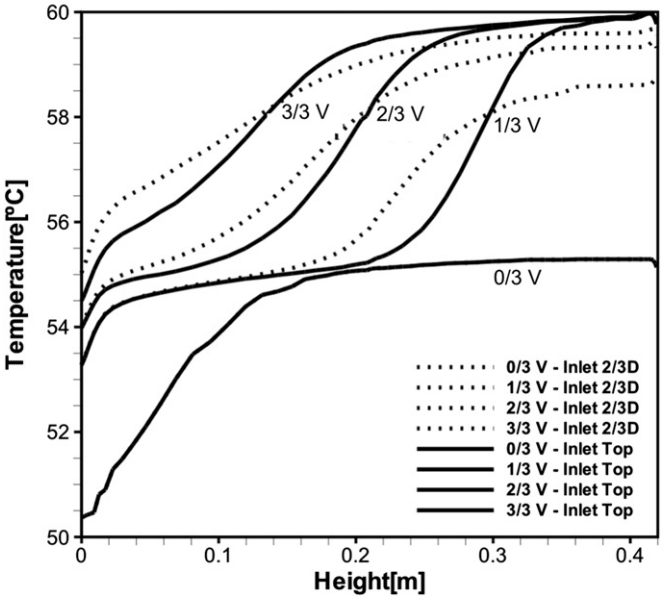

Fig. 17. Numerical temperature profiles for the cases of inlet jets located at 2/3*D* and next to the top for an intake of 78 l (3/3*V*).

shown in Fig. 12. The mesh and the boundary conditions were the same of the last case, but this time the inlet jet temperature was imposed as 8 °C above the water temperature in the exit of the tank, at the base. So, to make a comparison possible, the case with inlet jet located at 2/3 of diameter also was simulated for this boundary condition.

Fig. 16 presents the numerical temperature profiles for successive increments of 10 l of hot water, except for the last curve, corresponding to 1/3 of tank volume (26 l). For comparison, the curves obtained for the inlet jets located at 2/3 of the height are also shown. The numerical solution shows that the use of the inlet jet at the top of the tank led to a better thermal stratification when compared with the inlet jet placed at 2/3 of the height (tank diameter). Fig. 17 gives a comparison between these two cases, for additional incoming hot water volume equal to 2/3*V* and 3/3*V*.

Fig. 17 shows that the best stratification was attenuated by this additional intake of hot water, so that when the process completed one cycle (the circulated water was equal to the tank volume), the stratification profiles for both cases were closer. This behavior was caused due to the shape of the temperature profile applied as initial condition, because after the discharge of the thermally stratified layer, the water temperature discharged from the tank became approximately constant for the next times. Consequently, from this moment on, the temperature of the water entering the tank either through the top or at 2/3 of the height also became constant, although 8 °C higher due to the imposed boundary condition.

Based on these numerical results, the inlet jet near the top of the tank could be predicted only to allow a better thermal stratification, while the temperature of the water entering the tank was higher than the temperature of the water inside the tank at that same height. When the temperature of the inlet jet was maintained constant for a long period, the temperature of the water in the tank became very close to the temperature of the inlet jet, so that the advantage of the water intake through the top disappeared.

5. Conclusions

The developed three-dimensional computing code was able to accurately determine the velocity and temperature fields inside horizontal cylindrical storage tanks, subject to the heat loss to the environment, including cases with the presence of laminar jets. One correlation was proposed for thermal stratification degree and another to make possible to predict the temperature profile during the cooling process.

The correlation for the thermal stratification degree showed that the stratification degree increased as the heat loss increased. The proposed correlation to predict the temperature profile can be very useful in the study of many applications, such as in thermosiphon solar water heating systems, where this information can be used by engineers to design more efficient systems. Also, the temperature profile provided by this correlation can be used as a reference in the validation of mathematical models, for instance, considering a multinode approach.

The numerical investigations considering the storage tank connected to solar collectors showed that the presence of the baffle plate allows the formation of temperature profiles with a better thermal stratification, as long as the inlet jet temperature was significantly higher than the temperature of the water inside the tank at that same height. Also, the inlet jet next to the top was found to lead to a greater thermal stratification. However, it was verified that when the inlet jet temperature remains constant for a long period of time, so that the mean temperature at the height of the inlet approaches the temperature of inlet jet, the temperature profiles become similar to the case of inlet located at 2/3 of the diameter of the tank, without baffle plate. In this case, the announced advantage disappears.

Acknowledgements

This work has been developed under the sponsorship of the CNPq, the Brazilian government entity for scientific and technology development.

References

[1] Schneider S, Straub J. Laminar natural convection in a cylindrical enclosure with different end temperatures. Int J Heat Mass Transfer 1992;35:545–57.
[2] Eames PC, Norton B. The Effect of tank geometry on thermally stratified sensible heat storage subject to low reynolds number flow. Int J Heat Mass Transfer 1998;41:2131–42.
[3] Alizadeh S. An experimental and numerical study of thermal stratification in a horizontal cylindrical solar storage tank. Solar Energy 1999;66:409–21.
[4] Zachar A, Farkas I, Szlivka F. Numerical analyses of the impact of plates for thermal stratification inside a storage tank with upper and lower inlet flows. Solar Energy 2003;74:287–302.
[5] Oliveski RC, Krenzinger A, Vielmo HA. Cooling of cylindrical vertical tanks submitted to natural internal convection. Int J Heat Mass Transfer 2003;46: 2015–26.
[6] Oliveski RC, Krenzinger A, Vielmo HA. Comparison between models for the simulation of hot water storage tanks. Solar Energy 2003;75:121–34.
[7] Shah LJ, Furbo S. Entrance effects in solar storage tanks. Solar Energy 2003;75: 337–48.
[8] Consul R, Rodrigues I, Perez-Segarra CD, Soria M. Virtual prototyping of storage tanks by means of three-dimensional CFD and heat transfer numerical simulation. Solar Energy 2004;77:179–91.
[9] Duffie JA, Beckman WA. Solar engineering of thermal processes. John Wiley & Sons; 1991. p. 153.
[10] Savicki DL. Tridimensional numerical analysis and experimental investigation of the thermal and hydrodynamic behaviors of cylindrical storage tanks. Mechanical Engineering Graduate Program of the UFRGS, Doctoral thesis; 2007 [in Portuguese].
[11] Versteeg HK, Malalasekera. Introduction to computational fluid dynamics. London: Longman Scientific & Technical; 1995.
[12] Hayase T, Humphrey C, Greif R. A consistently formulated quick scheme for fast and stable convergence using finite-volume iterative calculation procedures. J Comput Phys 1992;98:108–18.
[13] Li Y, Rudmam M. Assessment of higher-order upwind schemes incorporating fct for linear and nonlinear convection-dominated problems. Numer Heat Transfer 1995;27:1–21.